We are IntechOpen, the world's leading publisher of Open Access books Built by scientists, for scientists

4,800
Open access books available

122,000
International authors and editors

135M
Downloads

Our authors are among the

154
Countries delivered to

TOP 1%
most cited scientists

12.2%
Contributors from top 500 universities

CLARIVATE ANALYTICS BOOK CITATION INDEX INDEXED

WEB OF SCIENCE™

Selection of our books indexed in the Book Citation Index in Web of Science™ Core Collection (BKCI)

Interested in publishing with us?
Contact book.department@intechopen.com

Numbers displayed above are based on latest data collected.
For more information visit www.intechopen.com

12

High PerformanceTracking Control of Automated Slewing Cranes

Frank Palis and Stefan Palis
Otto-von-Guericke-University Magdeburg
Germany

1. Introduction

Automation of slewing cranes in handling and transport processes is getting more and more important. However, each crane operation causes swaying movements of load, which are weakly damped. Therefore active damping of swaying movements is a major task in automated crane operation. The main difficulty here, in contrast to overhead travelling cranes, is the coupling between rotary and translation movements, which calls for a special approach when designing the control scheme.

Fig. 1. Slewing crane

There has been extensive research on active damping of overhead travelling cranes. Here, in most cases linear models are used and controlled in open loop operation via time or energy optimal control laws (Buch, 1999) or via feedback control for sway angle rejection (Palis, 1989). However, application of these strategy for slewing cranes raises difficulties because of non-linearity and complexity of motion. Publications on gantry cranes and boom cranes (Arnold et al., 2007) tackle this problem but here no complete model of load dynamics is given.
The actuator system of a slewing crane consists generally of an electrical drive system. Its control system is usually designed in cascade structure and optimized using linear standard

criteria (Betragsoptimum, symmetrical optimum) with P/PI-controllers. Current limitation is realized by current reference value limitation. Because of its easy implementation this structure is highly accepted in practice. Specific technological tasks can be taken into consideration by overlaid control loops that provide the appropriate reference values for the speed controlled drive system.

To this aim, as will be shown, crane motion can be separated into a rapid and a slow component according to the principle of motion decomposition. The rapid component is controlled by the high dynamic speed or position control loop able to reproduce the desired trajectory and to compensate for existing force interactions between the motion axis. The slow component describes load dynamics governed by the trajectory of the corresponding axis. As shown for overhead travelling cranes in (Palis, 1989) this approach facilitates considerably control system design and allows the use of standard speed controlled drive systems. Moreover, the proposed motion separation offers ideal possibilities for system linearization, adaptive control and flatness based trajectory tracking.

Mathematical description of slewing crane movement differs considerably from gantry cranes and overhead travelling cranes. Crane movement is characterized by the appearance of Coriolis and centrifugal forces. Consequently, the system of governing equations is becoming significantly non-linear and the application of linear control theory methods may lead to problems. Practical and simulation investigations prove that both components may considerably influence the movement of slewing cranes and that they must by taken into account when designing and optimizing the controller system. To solve this problem, three different approaches can be utilized:

- Consideration of parameter variations and non-linear force interactions via control parameter adaptation,
- Linearization of the plant via appropriate compensating loops and linearization of plant parameters and
- Application of robust control strategies able to guaranty satisfactory system behaviour in the whole range of working even if plant parameters are changing and Coriolis and centrifugal forces appear.

It is obvious that the first mentioned two methods starts from the supposition of a known and defined plant model. Here, the main problem consists in finding the complete system of governing equations to describe the load motion trajectory. In (Sawodny et al., 2002) a solution for a boom crane with hydraulic drive system is given where centripetal and Coriolis terms are neglected and the rope length is taken constant. Consequently, the obtained results cover only a limited range of applications. To generalize these results all significant force couplings and changing rope length have to be taken into account. The following investigations will show that these effects may lead to considerable deviations between motion of simplified models where these effects are neglected and the real load. Therefore, one of the main concerns of the paper will be the derivation of an complete mathematical model of the load trajectory for slewing cranes. It will be shown that the obtained relatively complex system of governing equations for the swinging load can be considerably simplified using the above mentioned principle of motion separation.

Due to the complexity of the load dynamics and starting from the supposition that handling tasks for slewing cranes do not require extremely high position nor travel trajectory accuracy the authors proposed in (Palis & Palis, 2005) a robust control strategy. These works were aimed at finding a control strategy that features robustness in the whole range of

possible parameter variations as well as Coriolis and centrifugal forces and which, in addition, guaranties necessary motion quality. To solve this task a LQ-controller was implemented without taking into consideration the mentioned nonlinear effects and force interactions. It was shown that this approach may be satisfying for many practical handling tasks. However, when more precise tracking performances are required more sophisticated control schemes are needed.

2. Nonlinear model of the slewing crane

To describe motion of the slewing crane, the equivalent kinematic scheme with concentrated masses represented in figure 2 is utilized. Hence, dynamics of the generalized rotating crane represents a multibody system with 5 independent degrees of freedom (DOF)

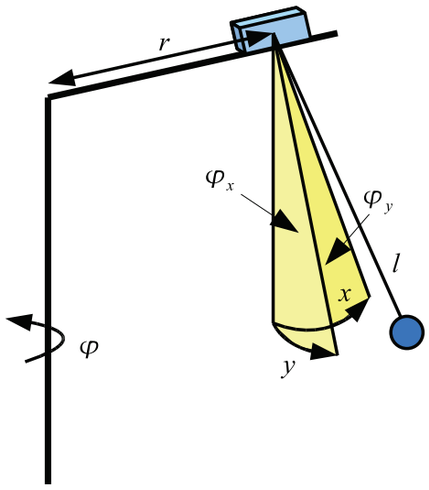

$q_1 = \varphi$ slewing gear rotation angle

$q_2 = r$ radial position of the trolley

$q_3 = l$ hoisting gear movement

$q_4 = \varphi_x$ sway angle in radial direction

$q_5 = \varphi_y$ sway angle perpendicular to the radial direction.

Fig. 2. Equivalent kinematic scheme

The task consists in load positioning along a desired trajectory with given accuracy using a position controlled drive system for the trolley, slewing and hoisting gear. Referring to the equivalent kinematic scheme the following energy balances can be established:

- the potential energy of the load,

$$V = m_L g l\left(1 - \cos\varphi_x \cos\varphi_y\right) \tag{1}$$

- the kinetic energy of the tower T_T, the boom T_B, the trolley T_R and the load T_L.

$$T_T = \frac{1}{2} J_T \dot{\varphi}^2 \tag{2}$$

$$T_B = \frac{1}{2} m_B r_B^2 \dot{\varphi}^2 \tag{3}$$

$$T_R = \frac{1}{2} m_R \left(r^2 \dot{\varphi}^2 + \dot{r}^2\right) \tag{4}$$

$$T_L = \frac{1}{2} m_L \left[\begin{array}{l} \left(\begin{array}{l} -\dot{\varphi}\sin\varphi\left(-\sin\varphi_x + r\right) + \cos\varphi\left(\dot{l}\sin\varphi_x + \dot{\varphi}_x l\cos\varphi_x + \dot{r}\right) \\ -\dot{l}\sin\varphi\sin\varphi_y - l\dot{\varphi}\cos\varphi\sin\varphi_y - l\dot{\varphi}_y\sin\varphi_y\cos\varphi_y \end{array} \right)^2 \\ + \left(\begin{array}{l} \dot{\varphi}\cos\varphi\left(l\sin\varphi_x + r\right) + \sin\varphi\left(\dot{l}\sin\varphi_x + l\dot{\varphi}_x\cos\varphi_x + \dot{r}\right) \\ +\dot{l}\cos\varphi\sin\varphi_y - l\dot{\varphi}\sin\varphi\sin\varphi_y + l\dot{\varphi}_y\cos\varphi \end{array} \right)^2 \\ + \left(\dot{l}\cos\varphi_x\cos\varphi_y - l\dot{\varphi}_x\sin\varphi_x\cos\varphi_y - l\dot{\varphi}_y\cos\varphi_x\sin\varphi_y\right)^2 \end{array} \right] \tag{5}$$

Establishing the Lagrange function

$$L = T - V \tag{6}$$

and applying the Lagrange formalism

$$\frac{d}{dt}\left(\frac{\partial L}{\partial \dot{q}_i}\right) - \frac{\partial L}{\partial q_i} = Q_i \tag{7}$$

we obtain the system of governing equations with the generalized coordinates q_i that can be written in the general form.

$$Q = D(q)\ddot{q} + C(q,\dot{q}) + G(q) \tag{8}$$

Figure 3 depicts equation (8) with

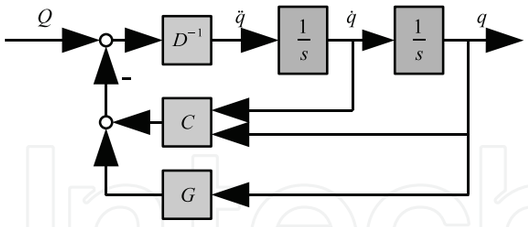

Q	generalized actor forces
q	generalized coordinates
$\mathbf{C = C_{centr} + C_{cor}}$	coupling matrix to calculate Coriolis and centrifugal effects respectively
G	gravitation matrix

Fig. 3. General scheme of motion

The exact calculation using eq. (5) leads to very large and complex expressions difficult to interpret physically and inconvenient to implement practically. To simplify the system of governing equations we take into account that only small sway angles are admitted. Consequently the following assumptions can be made.

$$\begin{array}{l} \sin\varphi_x \approx \varphi_x,\ \sin\varphi_y \approx \varphi_y,\ \cos\varphi_x \approx 1,\ \cos\varphi_y \approx 1 \\ \sin^2\varphi_x \approx \sin^2\varphi_y \approx \sin\varphi_x\sin\varphi_y \approx 0 \\ \varphi_y\ddot{\varphi}_x \approx \varphi_x\ddot{\varphi}_y \approx \varphi_y\dot{\varphi}_y \approx \varphi_x\dot{\varphi}_x \approx \dot{\varphi}_x\dot{\varphi}_y \approx \varphi_x\dot{\varphi}_y \approx \varphi_y\dot{\varphi}_x \end{array} \tag{9}$$

With these simplifying assumptions the respective terms of eq. (3) can be specified

$$\mathbf{D}(\mathbf{q})\ddot{q} = \left[\begin{array}{ccc:cc} (m_K + m_L) & -m_L l\varphi & m_L\varphi_x & m_L l & 0 \\ -m_L l\varphi_x & J_H & m_L r\varphi_y & 0 & m_L rl \\ m_L\varphi_x & 0 & m_L & 0 & 0 \\ \hdashline 1 & -l\varphi_y & 0 & l & 0 \\ 0 & (r + l\varphi_x) & 0 & 0 & l \end{array}\right] \left[\begin{array}{c} \ddot{r} \\ \ddot{\varphi} \\ \ddot{l} \\ \hdashline \ddot{\varphi}_x \\ \ddot{\varphi}_y \end{array}\right] = \left[\begin{array}{c:c} \mathbf{A_1} & \mathbf{D_1} \\ \hdashline \mathbf{D_2} & \mathbf{A_2} \end{array}\right] \left[\begin{array}{c} \ddot{r} \\ \ddot{\varphi} \\ \ddot{l} \\ \hdashline \ddot{\varphi}_x \\ \ddot{\varphi}_y \end{array}\right] \tag{10}$$

$$\mathbf{C}(\mathbf{q},\dot{\mathbf{q}}) = \left[\begin{array}{c} -m_L(r + l\varphi_x) - m_K r \\ 0 \\ -m_L r\varphi_x \\ \hdashline -(r + l\varphi_x) \\ -l\varphi_y \end{array}\right] \dot{\varphi}^2 + 2 \left[\begin{array}{c} m_L\left(-\dot{l}\dot{\varphi}_x + \varphi_y \dot{l}\dot{\varphi} + l\dot{\varphi}\dot{\varphi}_y\right) \\ m_L(r\dot{l}\dot{\varphi}_y + \varphi_x r\dot{\varphi}\dot{l} + rl\dot{\varphi}\dot{\varphi}_x + r\dot{r}\dot{\varphi} + l\varphi_x\dot{\varphi}\dot{r}) + m_K r\dot{r}\dot{\varphi} \\ m_L\varphi_y \dot{r}\dot{\varphi} \\ \hdashline \dot{l}\dot{\varphi} - l\dot{\varphi}\dot{\varphi}_y - \varphi_y\dot{l}\dot{\varphi} \\ l\dot{\varphi}\dot{\varphi}_x + \dot{\varphi}\dot{r} + \dot{l}\dot{\varphi}_y + \varphi_x\dot{l}\dot{\varphi} \end{array}\right] \tag{11}$$

$$\mathbf{C}(\mathbf{q},\dot{\mathbf{q}}) = \left[\begin{array}{c} \mathbf{C}_{\mathbf{cent},1} \\ \hdashline \mathbf{C}_{\mathbf{centr},2} \end{array}\right] \dot{\varphi}^2 + \left[\begin{array}{c} \mathbf{C}_{\mathbf{cor},1} \\ \hdashline \mathbf{C}_{\mathbf{cor},2} \end{array}\right] \tag{12}$$

with

$$J_H = m_K r^2 + m_L\left(r + l\varphi_x\right)^2 + m_T r_a^2 + J_T \tag{10}$$

$$\mathbf{Q} = \left[F_K \quad M \quad F_H \,\vdots\, 0 \quad 0\right]^T = \left[\begin{array}{c} \mathbf{Q_1} \\ \hdashline \mathbf{0} \end{array}\right] \tag{14}$$

$$\mathbf{G} = \left[0 \quad 0 \quad g \,\vdots\, -g\varphi_x \quad -g\varphi_y\right]^T = \left[\begin{array}{c} \mathbf{G_1} \\ \hdashline \mathbf{G_2} \end{array}\right] \tag{15}$$

3. System decomposition

3.1 Fast subsystem (drive control system) and slow subsystem (swinging load)

From equations (10)-(15) can be drawn the conclusion that the overall system can be formally decomposed into 2 subsystems governing the DOF $\mathbf{q_1} = \left[r \quad \varphi \quad l\right]^T$ and $\mathbf{q_2} = \left[\varphi_x \quad \varphi_y\right]^T$ described by the following equations.

$$\left[\begin{array}{c} \mathbf{Q_1} \\ \hdashline \mathbf{Q_2} \end{array}\right] = \left[\begin{array}{c} \mathbf{A_1}\ddot{\mathbf{q}}_1 + D_1\ddot{\mathbf{q}}_2 \\ \hdashline \mathbf{D_2}\ddot{\mathbf{q}}_1 + \mathbf{A_2}\ddot{\mathbf{q}}_2 \end{array}\right] + \left[\begin{array}{c} \mathbf{C}_{\mathbf{ce1}} \\ \hdashline \mathbf{C}_{\mathbf{ce2}} \end{array}\right] \dot{\varphi}^2 + \left[\begin{array}{c} \mathbf{C}_{\mathbf{co1}} \\ \hdashline \mathbf{C}_{\mathbf{co2}} \end{array}\right] + \left[\begin{array}{c} \mathbf{G_1 q_1} \\ \hdashline \mathbf{G_2 q_2} \end{array}\right] \tag{16}$$

Both subsystems are graphically represented in fig. 4.

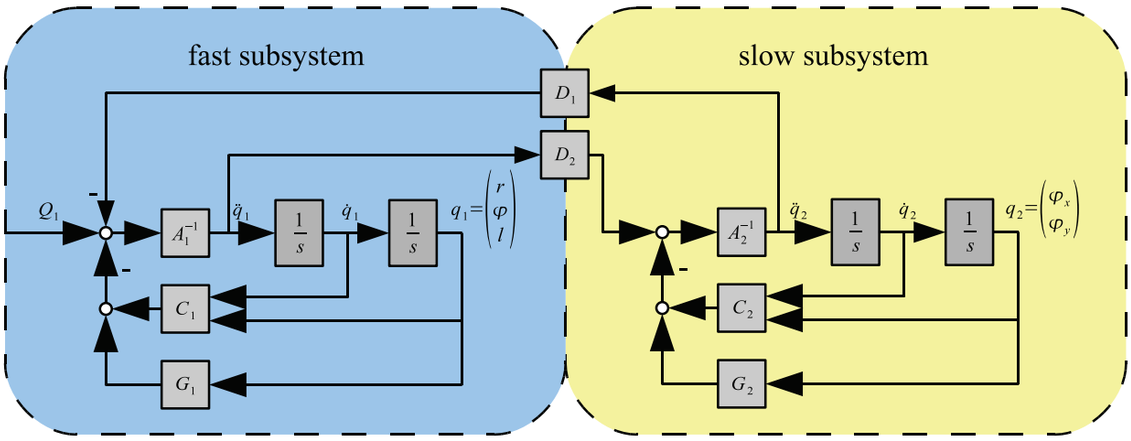

Fig. 4. System decomposition

On the supposition that a speed or position controlled electric drive system is utilized the fast subsystem in fig. 4 must be extended by introducing inner current and speed and outer position control loops. Fig. 5 depicts the drive related fast subsystem for the coordinates $\mathbf{q_1} = \begin{bmatrix} r & \varphi & l \end{bmatrix}^T$.

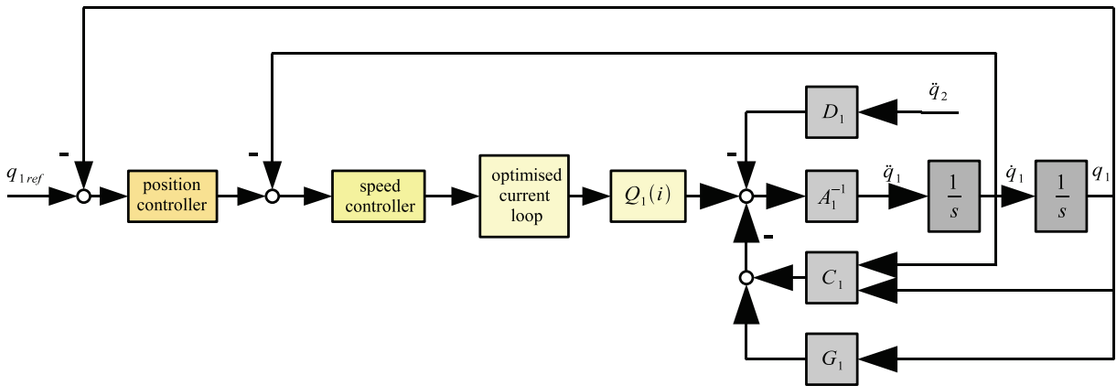

Fig. 5. Speed and position controlled electric drive system

In accordance with the rules of cascade structure systems commonly used in drive systems the time constant of the inner current loop determines the dynamics of the overall system. Assuming a time constant of $(1...2)ms$ for the current loop, speed and position control reactions are much more faster than load dynamics. Therefore all force couplings affecting the drive system are compensated by the speed controller. To improve dynamics of the speed control system related to these couplings well known disturbance observers or decoupling networks can be used. Assuming the above discussed structural conditions system dynamics can be decomposed into the two subsystems as assumed above. The first subsystem is characterized by the fast drive control system with the output variables $\mathbf{q_1}$, whereas the second subsystem reflects the dynamics of the relatively slow load swinging governed by the output of the fast subsystem $\ddot{\mathbf{q}}_1$. Due to their difference in dynamics both systems can be considered separately what significantly facilitates control design. Strictly

speaking, the matrix $\mathbf{A}_1$ is affected by the output of the slow subsystem $\mathbf{q_2} = \begin{bmatrix} \varphi_x & \varphi_y \end{bmatrix}^T$. However, due to small sway angles and its slow changes matrix $\mathbf{A}_1$ can be taken constant.

3.2 Transformation of the slow subsystem and damping strategy

It is obvious that the slow system depicted in fig. 4 is governed by the acceleration of the fast position controlled drive system. Hence, any control signal to damp the swinging load must be transformed into the corresponding position signal. To this aim the governing equation of the slow subsystem in equation (16) must be integrated. The velocity governed subsystem yields

$$\int \mathbf{D_2}\ddot{\mathbf{q}}_1 dt + \int \mathbf{A_2}\ddot{\mathbf{q}}_2 dt + \int \mathbf{C}_2 dt - \int g\mathbf{q_2} dt = \mathbf{0} \tag{11}$$

and the position governed subsystem is described by

$$\iint \mathbf{D}_2\ddot{\mathbf{q}}_1 dt^2 + \iint \mathbf{A}_2\ddot{\mathbf{q}}_2 dt^2 + \iint \mathbf{C}_2 dt^2 - \iint g\mathbf{q}_2 dt^2 = \mathbf{0} \tag{12}$$

Neglecting the time dependence of $\mathbf{D}_2$ and $\mathbf{A}_2$ leads to a simplified system of equations with a given error $\boldsymbol{\Delta}$ for the velocity governed subsystem

$$\mathbf{D_2}\dot{\mathbf{q}}_1 + \mathbf{A_2}\dot{\mathbf{q}}_2 + \int \mathbf{C_2} dt - g\int \mathbf{q_2} dt + \boldsymbol{\Delta}_{\dot{q}} = \mathbf{0} \tag{13}$$

and the position governed subsystem

$$\mathbf{D_2}\mathbf{q}_1 + \mathbf{A_2}\mathbf{q}_2 + \iint \mathbf{C}_2 dt^2 - g\iint \mathbf{q}_2 dt^2 + \boldsymbol{\Delta}_q = \mathbf{0} \tag{14}$$

Equation (20) is represented in fig. 6 and leads to the conclusion that to damp this system we have to apply a negative feedback $\int \mathbf{q_2} dt$ to the position loop of the fast system.

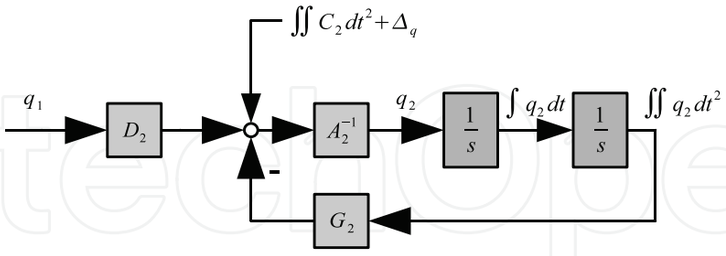

Fig. 6. Position controlled swinging load

Figure 7 illustrates how this feedback signal can be generated from the velocity governed model using the well known observer principle. Here we start from the supposition that the acceleration governed model of the slow system can be easily obtained taking into account all existing force couplings according to fig. 4.

This model is taken as reference model and its sway angles serve as fix point to adapt the simplified velocity governed model (19) where the coupling forces and the error due to the non-exact integration are taken into account via additive model correction. Hence, the simplified velocity governed model reflects all variables with high accuracy.

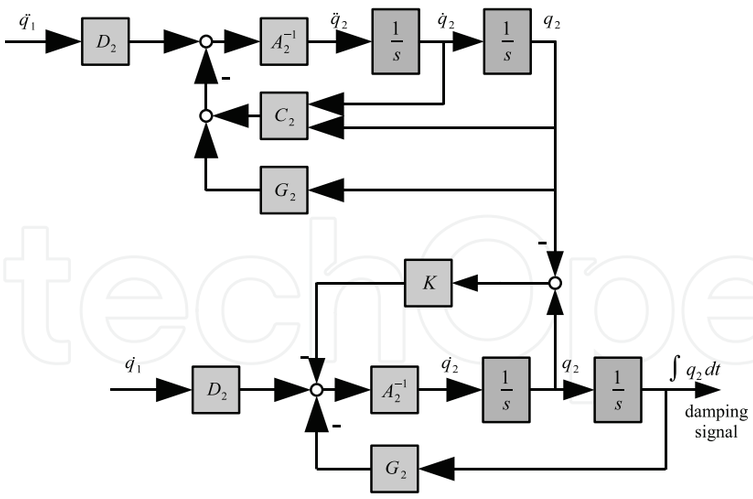

Fig. 7. Observer structure for deriving the damping signal

4. Strategy of sway angle rejection

Figure 8 depicts the general scheme for the proposed damping strategy. The sway angle is modelled based on the acceleration governed model of the slow system taking into consideration all significant couplings, force interactions and changing rope length. Using

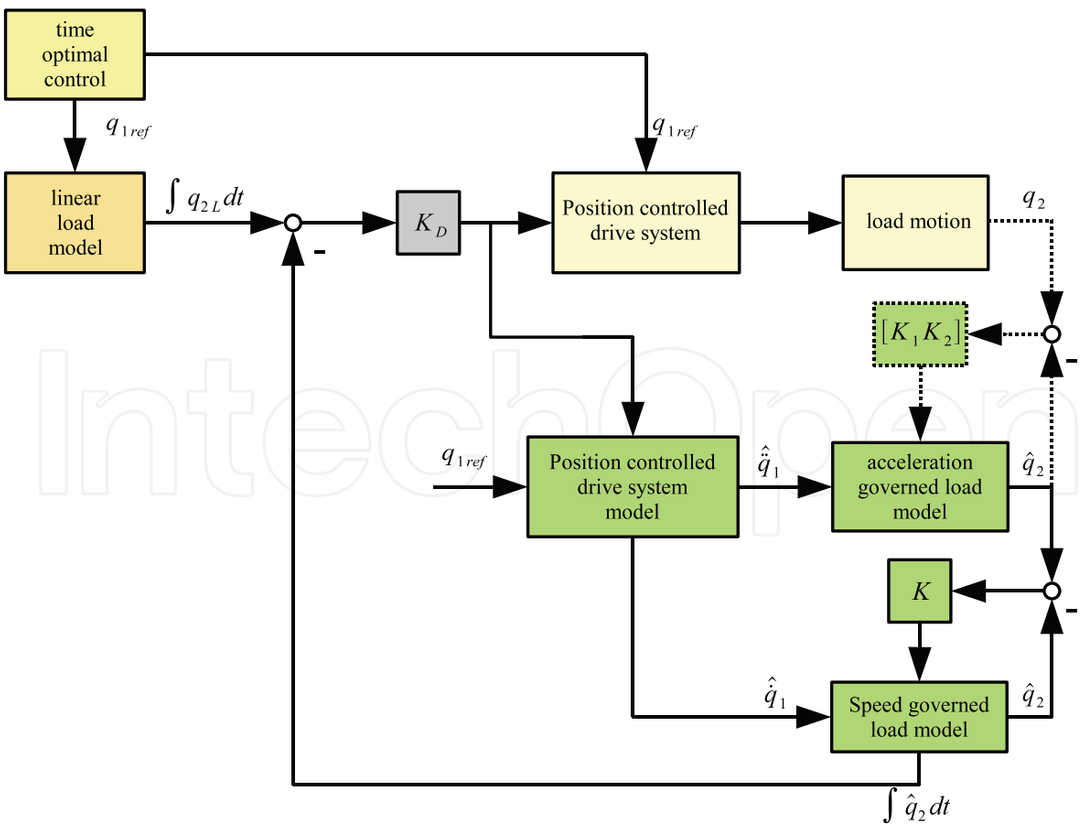

Fig. 8. General control scheme

state observer structure the acceleration governed load model is transformed into the velocity governed load model in order to determine the damping signal $\int \hat{\mathbf{q}}_2 dt$, that is applied to the position controlled drive system. The advantage of the model based approach consists in the fact that all effects like changing rope length, Coriolis and centrifugal forces can be taken into consideration. Hence, in some cases no measurement of the sway angles is needed and the system can work in open loop operation. However, it is obvious that in open loop operation external forces like e.g. wind forces and non-zero initial conditions of the angles are not reflected by the model. Here measurement is needed to correct the model variables as shown in fig. 8 by the dotted line. But even in these cases the model approach is necessary to generate the damping signal avoiding open integration of $\hat{\mathbf{q}}_2$. Moreover the model possesses good smoothing capacities so measurement disturbances can be filtered.
As known, damping leads to a prolongation of the acceleration and breaking phase of the positioning. To overcome this shortage a time or energy optimal control law for the linear load model with constant rope length is calculated (Buch, 1999) and applied to the velocity governed linear load model to determine its damping signal $\int \hat{\mathbf{q}}_{2L} dt$. The difference between this signal and the damping signal of the nonlinear load model $\int \hat{\mathbf{q}}_2 dt$ gives an error, which is applied through the scaling parameter K_D to the position controlled drive system. Hence, the presented damping strategy has an effect only on the deviation between the real load trajectory or trajectory of the nonlinear model and the optimal linear load trajectory. Consequently, a given load sway necessary to bring the load into the target position without final swaying in an optimal way is deducted from the damping algorithm.

5. Simulation results

5.1 Open loop system simulation

Figure 9 depicts the load trajectory in bird's eye view in open loop operation when a time optimal control law designed for the linear load model is applied. It is obvious that in this

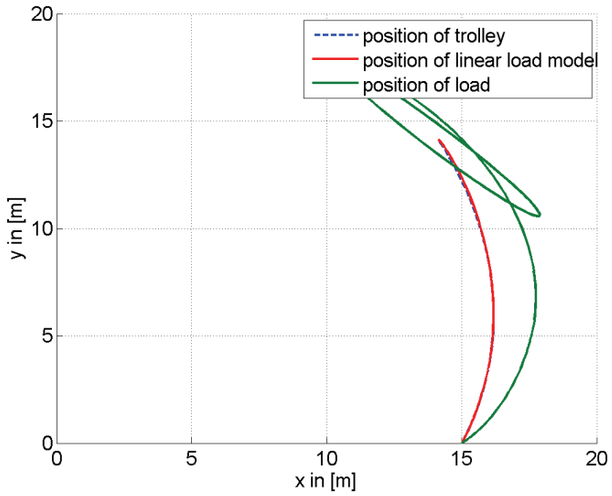

Fig. 9. Bird's eye view of load motion in open loop operation

case the load reaches its final position without swaying (red line). In contrast to this coupling forces and nonlinear system dynamics of the slewing crane lead to considerable deviations from the time optimal trajectory and to significant oscillations around the target position (green line). Figure 10 shows the motion as function of time for x and y in the global coordinate frame. Figure 11 depicts the same motion in the local coordinate frame attached to the trolley (fig. 2).

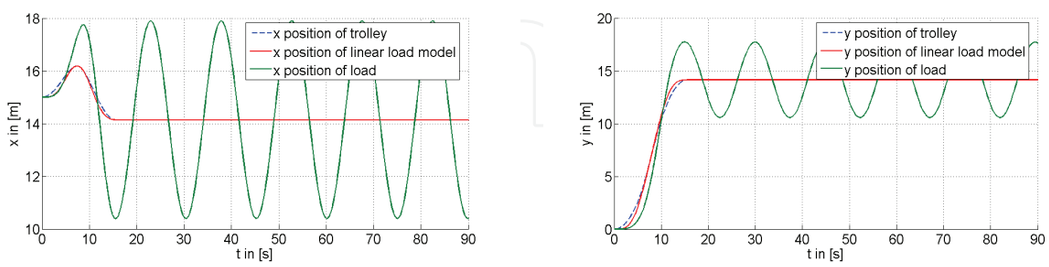

Fig. 10. Load motion in open loop operation as function of time in the global coordinate frame

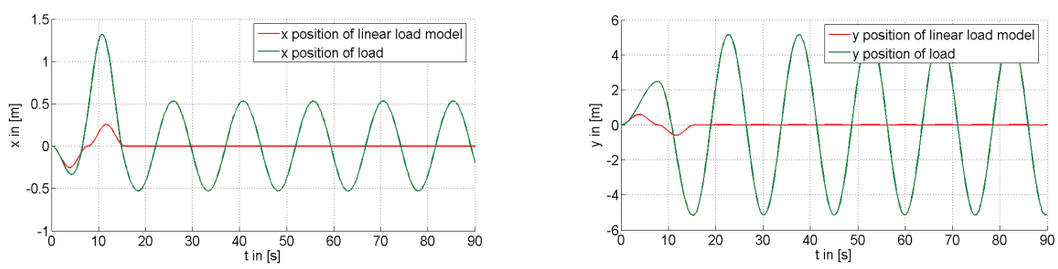

Fig. 11. Load motion in open loop operation as function of time in the local coordinate frame attached to the trolley

4.1 Closed loop system simulation

Figure 12 shows the load trajectory in bird's eye view in closed loop operation when the time optimal control is superposed by the proposed damping strategy. As can be seen

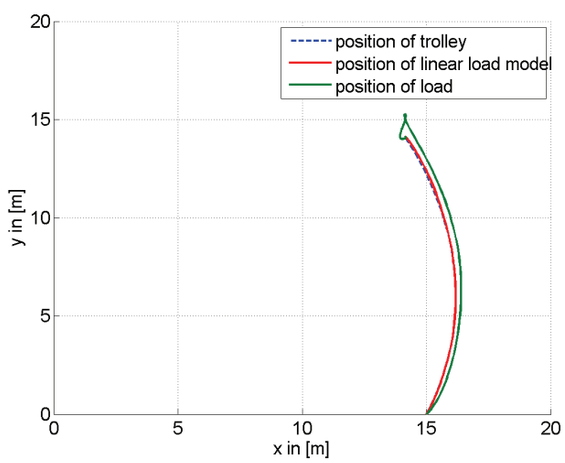

Fig. 12. Bird's eye view of load motion in closed loop operation

deviations from the time optimal trajectory are considerably reduced and swaying around the target position is completely rejected (green line). Figure 13 illustrates the motion in the global coordinate frame x and y over time. Figure 4 depicts the same motion in the local coordinate frame.

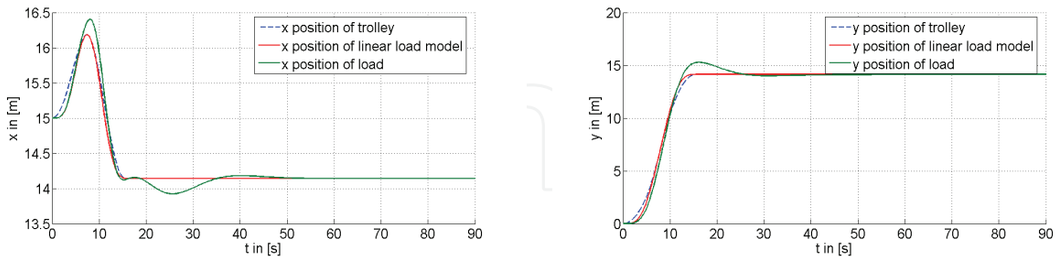

Fig. 13. Load motion in closed loop operation as function of time in the global coordinate frame

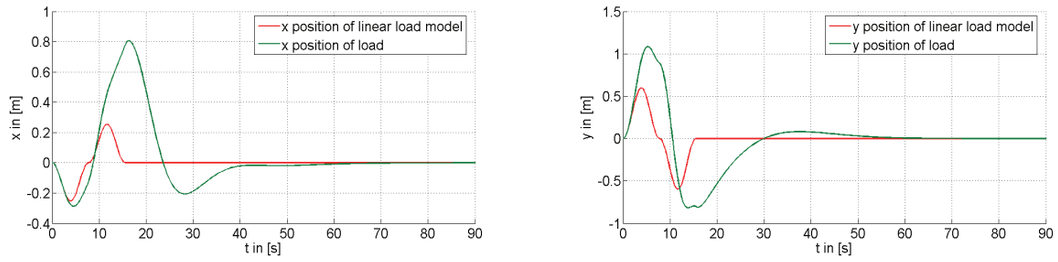

Fig. 14. Load motion in closed loop operation as function of time in the local coordinate frame attached to the trolley

5. Conclusion

Slewing crane motion is affected by nonlinear effects as Coriolis and centrifugal forces and couplings. A mathematical model containing all relevant effects and couplings under mild assumptions has been derived. Due to the difference in dynamics the general motion can be decomposed into a slow and fast subsystem, which can be optimized independently. The slow system reflects load dynamics and serves as basis for designing the proposed damping strategy. Promising simulation results have been obtained. Future investigations will focus on deriving optimal control laws for the nonlinear model and implementation and practical verification of the presented approach on a slewing crane.

6. References

Arnold, E.; Neupert, J. & Sawodny, O. (2007). Trajectory Tracking for Boom Cranes Based on Nonlinear Control and Optimal Trajectory Generation, *Proceedings of Control Applications*, pp.1444-1449, ISBN: 1085-1992, Singapore, Oct. 2007, Singapore

Sawodny, O.; Aschemann, H.; Kumpel, J.; Tarin, C. & Schneider, K. (2002). Anti-sway control for boom cranes, *Proceedings of American Control Conference*, pp. 244-249 vol. 1, ISBN: 0-7803-7298-0, Alaska, May 2002, Anchorage

Kim, Y. S.; Hong, K. S. & Sul, S.K., R. (2001). Anti-Sway Control of Container Cranes: Inclinometer, Observer and State Feedback. *International Journal of Control, Automation and Systems,* Vol. 2., No. 4, (December 2004) pp. 435-449

Palis, S.; Palis, F.; Lehnert M. (2005). Anti-Sway System for Slewing Cranes. *Proceedings of 22nd International Symposium on Automation and Robotics in Construction ISARC 2005*, Italy, Sept. 2005, Ferrara

Buch, A. (1999). *Optimale Bewegungssteuerung von schwingungsfähigen mechatronischen Systemen mit zwei Freiheitsgraden am Beispiel eines Krans mit pendelnder Last und elastischer Mechanik.* University of Magdeburg, Faculty of Electrical Engineering. Dissertation.

Palis, F. (1989). *Prozessangepasste Steuerung von elektrischen Kranantrieben mit Mikrorechnern.* Universität Magdeburg, Fakultät für technische Wissenschaften. Habilitationsschrift

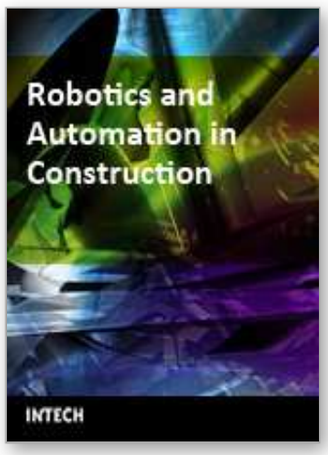

Robotics and Automation in Construction

Edited by Carlos Balaguer and Mohamed Abderrahim

ISBN 978-953-7619-13-8
Hard cover, 404 pages
Publisher InTech
Published online 01, October, 2008
Published in print edition October, 2008

This book addresses several issues related to the introduction of automaton and robotics in the construction industry in a collection of 23 chapters. The chapters are grouped in 3 main sections according to the theme or the type of technology they treat. Section I is dedicated to describe and analyse the main research challenges of Robotics and Automation in Construction (RAC). The second section consists of 12 chapters and is dedicated to the technologies and new developments employed to automate processes in the construction industry. Among these we have examples of ICT technologies used for purposes such as construction visualisation systems, added value management systems, construction materials and elements tracking using multiple IDs devices. This section also deals with Sensorial Systems and software used in the construction to improve the performances of machines such as cranes, and in improving Human-Machine Interfaces (MMI). Authors adopted Mixed and Augmented Reality in the MMI to ease the construction operations. Section III is dedicated to describe case studies of RAC and comprises 8 chapters. Among the eight chapters the section presents a robotic excavator and a semi-automated façade cleaning system. The section also presents work dedicated to enhancing the force of the workers in construction through the use of Robotic-powered exoskeletons and body joint-adapted assistive units, which allow the handling of greater loads.

InTech Europe
University Campus STeP Ri
Slavka Krautzeka 83/A
51000 Rijeka, Croatia
Phone: +385 (51) 770 447
Fax: +385 (51) 686 166

InTech China
Unit 405, Office Block, Hotel Equatorial Shanghai
No.65, Yan An Road (West), Shanghai, 200040, China
中国上海市延安西路65号上海国际贵都大饭店办公楼405单元
Phone: +86-21-62489820
Fax: +86-21-62489821

IntechOpen

IntechOpen